DOI: https://doi.org/10.2138/am-2020-7409. http://www.minsocam.org/

Revision 2 Correction 1

Titanium in calcium amphibole: behaviour and thermometry

Yue Liao [a], Chunjing Wei [a,*], Hafiz Ur Rehman [a,b]

[a] *MOE Key Laboratory of Orogenic Belts and Crustal Evolution, School of Earth and Space Sciences, Peking University, Beijing 100871, China*

[b] *Graduate School of Science and Engineering, Kagoshima University, Korimoto 1-21-35, Kagoshima 890-0065, Japan*

*Corresponding author: Chunjing Wei
Tel: +86 13651355549
Email address: cjwei@pku.edu.cn

DOI: https://doi.org/10.2138/am-2020-7409. http://www.minsocam.org/

Abstract

Thermometry of high-grade metamorphic rocks is difficult due to fast cationic diffusion during slow cooling, but the titanium content of calcium amphibole (Ti-Amp) can retrieve amphibole-forming temperature as high as ~1000 ºC. Based on pseudosection modelling and past research survey, we find that Ti-Amp is controlled by temperature under the conditions of oxygen fugacity less than 2 log units above the Ni-NiO oxygen buffer (ΔNNO ≤ 2), in subalkaline systems, and with the presence of Ti-phases (rutile, ilmenite or titanite). We apply available experimental data to calibrate a new Ti-Amp thermometer for such conditions:

$$T(°\mathrm{C}) = \frac{2400}{1.52 - \log \mathrm{Ti}^{\mathrm{Amp}}} - 273$$

where *T* is temperature and log $\mathrm{Ti}^{\mathrm{Amp}}$ is the Ti content of amphibole in atom per formula unit (apfu) expressed in the logarithm to base 10. The standard error of the calibration experiments is ±35 ºC. This thermometer can be applied only if the aforementioned conditions are fulfilled. Besides, caution should be taken when applying the thermometer to rocks under subsolidus water-unsaturated conditions, which can be observed as non-equilibrium textures or low bulk-rock water content (< 1–1.5 wt%). The results of this thermometer may be underestimated if applied to rocks that are equilibrated above 850 ºC, and contain rutile and a significant amount of water (> 3.5–4 wt%).

The new thermometer can be successfully applied to amphibole-bearing natural igneous and metamorphic rocks. In addition, we propose the Si *vs.* Ti in amphibole diagram that roughly demarcates the boundaries among the high amphibolite, high-temperature granulite, and ultrahigh-temperature granulite facies. Although pseudosection modelling provides details of the *P-T* evolution of studied rocks, the Ti-Amp thermometer is quick and easy to apply. However, further research is needed to improve our knowledge on the behaviour and stability of

amphibole, and to improve the accuracy of both pseudosection modelling and conventional thermometry.

Keywords: Thermometer, titanium in calcium amphibole, granulite, amphibolite, igneous rocks, pseudosection

Introduction

High-grade metamorphic rocks usually experience slow cooling processes at relatively high temperature. Fast component diffusion during high-temperature cooling boosts compositional resetting, causing great difficulties in estimating peak temperature (Frost and Chacko, 1989; Pattison et al., 2003). There are several examples of natural rocks metamorphosed at >900 ºC (e.g. Harley, 1989, 1998; Li and Wei, 2016; Santosh et al., 2007), so thermometric methods with high closure temperature are required for such conditions. For example, diagnostic assemblages such as sapphirine-quartz and sillimanite-orthopyroxene in ultrahigh-temperature (UHT) metapelite are resistant to destruction during slow cooling (Frost and Chacko, 1989; Harley, 1989). Rare-earth-element-based thermometers on certain minerals have also been successfully applied to high-temperature (HT) and UHT metamorphic conditions (Liu and Wei, 2018; Yang and Wei, 2017).

Calcium amphibole is one of the most common minerals that crystallize/recrystallize in hydrated igneous rocks, amphibolites and mafic granulites, and can be stable up to 950–1100 ºC (e.g. Rushmer, 1993; Sen and Dunn, 1994; Springer and Seck, 1997; Wyllie and Wolf, 1993). Lots of efforts have been made to establish amphibole-related thermometers. The classical amphibole-plagioclase thermometers of Holland and Blundy (1994) use exchange of (NaAl)(□Si)$_{-1}$ or (NaSi)(CaAl)$_{-1}$ (Spear, 1980, 1981). However, amphibole and plagioclase are commonly zoned; in equilibrium, sometimes amphibole grows with plagioclase breaking down during suprasolidus cooling (e.g. Koester et al., 2002; Palin et al., 2016; Rapp and Watson, 1995; Skjerlie and Johnston, 1996; Springer and Seck, 1997); and plagioclase hardly re-equilibrates once formed (Spear and Florence, 1992). Thus the application of these thermometers needs care, ensuring that the textural equilibrium between amphibole and plagioclase was reached (Blundy and Cashman, 2008). Moreover, these thermometers may not be available to rocks with amphibole Mg# [= Mg/(Mg + Fe_{total})] > 0.5 (Blundy and Cashman, 2008). There are also several amphibole-liquid thermometers (Molina et al., 2015; Putirka, 2016), but the required chemical composition of coexisting melts is hard to quantify in some cases. Moreover, some amphibole-only multi-component thermometers (Putirka, 2016; Ridolfi and Renzulli, 2012; Ridolfi et al., 2010) were successfully applied to igneous systems, but have unpredictable uncertainties for slow-cooling rocks due to the involvement of fast-diffusing cations like K, Na and Fe.

The titanium content of amphibole (Ti-Amp) tends to increase with temperature (Bard, 1970; Helz, 1973; Raase, 1974). Otten (1984) proposed a Ti-Amp thermometer for the conditions with oxygen fugacity (fO_2) near the quartz-fayalite-magnetite (QFM) buffer and Ti buffered by ilmenite, based on a limited number of experiments conducted by Helz (1973). In addition, Ernst and Liu (1998) proposed a semi-quantitative Ti-Amp thermometer for mid-ocean-ridge basalt (MORB) that contained amphibole coexisting with Ti-phases under conditions of fO_2 near QFM. Liao and Wei (2019) recovered peak temperatures of ~1000 ºC from the natural mafic granulites of the Huai'an Complex, North China Craton, using Ti-Amp isopleths in pseudosection modelling. These results indicate low diffusion rates of Ti-Amp in the studied rocks, and provide encouraging prospects for the application of Ti-Amp thermometry in slow-cooling rocks. Mongkoltip and Ashworth (1983) found resetting of Ti-Amp due to exsolution of ilmenite and rutile in amphibole in slow-cooling intrusions, possibly resulting from the low diffusion rates of Ti-Amp. However, Ti-Amp is not only controlled by temperature, but can be reduced by high fO_2 (Helz, 1973), or elevated in alkaline systems (Molina et al., 2009). Based on the above lines of inferences, Ti-Amp seems to be a promising thermometer, but its applicable conditions need further discussion and redefinition. In this study, we discuss Ti-Amp behaviour using pseudosection modelling, and propose a new Ti-Amp thermometer based on experimental constraints. Mineral abbreviations used throughout the text are after Whitney and Evans (2010), the classification of amphibole follows Hawthorne et al. (2012), and Ti-phases include rutile, ilmenite and titanite.

Ti-Amp behaviour based on pseudosection modelling

We discuss Ti-Amp behaviour using pseudosection modelling. The modelling calculations are performed in the system Na_2O-CaO-K_2O-FeO-MgO-Al_2O_3-SiO_2-H_2O-TiO_2-Fe_2O_3 (NCKFMASHTO) using THERMOCALC 3.45 based on Powell et al. (1998), with the internally consistent thermodynamic dataset (ds62) of Holland and Powell (2011). The set of activity-composition models include metabasite melt, augitic clinopyroxene, hornblendic amphibole (Green et al., 2016), orthopyroxene, garnet, biotite, muscovite (White et al., 2014), plagioclase (Holland and Powell, 2003), epidote (Holland and Powell, 2011), ilmenite/hematite (White et al., 2000) and endmember phases (quartz, rutile, titanite).

***P-T* pseudosections for MORB composition**

We perform *P-T* pseudosection modelling for the MORB composition used in Palin et al. (2016) (H_2O = 1.8 wt%, Fe^{3+}/Fe_{total} = 0.12) as an example to investigate the correlation of Ti-Amp with the factors involving temperature, pressure, and mineral assemblage. Although Green et al. (2016) recommended their metabasite set to be applied to the conditions of < 1.3 GPa, we

DOI: https://doi.org/10.2138/am-2020-7409. http://www.minsocam.org/

slightly expand pressure to 1.5 GPa (Fig. 1a). Amphibole is present throughout the system except under conditions of >1.3 GPa and >950 ºC, and higher temperature conditions for lower pressures. The water-saturated solidus temperature is 610 ºC at 1.1 GPa, and increases to ~700 ºC under higher or lower pressure conditions. Garnet is present at > 1.0 GPa for temperature > 850 ºC, but its presence requires higher pressure at lower temperature. Orthopyroxene is present at approximately >850 ºC / <1.0 GPa. Plagioclase is stable throughout the *P*-*T* field. The stability fields of rutile, ilmenite and titanite slightly overlap. Ilmenite is mainly present at >800 ºC / <0.9 GPa, rutile at >800 ºC / >0.9 GPa, and titanite at <800 ºC. The water-saturation curve lies alongside the solidus with the deliberately set water content.

Moreover, we replot the pseudosection with metamorphic facies in Fig. 1b. The UHT granulite facies covers the field with temperature > 900 ºC with the presence of orthopyroxene. The HT granulite facies field is defined based on the presence of orthopyroxene at < 900 ºC. The garnet amphibolite facies and the high-pressure granulite facies are defined by the presence of garnet, clinopyroxene and plagioclase at < 900 ºC, but the differences between them are not defined strictly here. The high amphibolite facies corresponds to the suprasolidus field with amphibole, plagioclase but no orthopyroxene, whereas the low amphibolite facies refers to the subsolidus field with similar assemblages. The eclogite facies corresponds to the plagioclase-absent field in the upper-left corner.

As is shown in Fig. 1, Ti-Amp isopleths are near-parallel to the pressure axis for most assemblages. Temperatures of the isopleths are lowest around 0.8–1.0 GPa, but gradually increase at higher and lower pressures. These results indicate that Ti-Amp is strongly temperature-dependent, but its slight pressure-dependence is also observed.

DOI: https://doi.org/10.2138/am-2020-7409. http://www.minsocam.org/

T-X pseudosections for subalkaline mafic rocks

To discuss the influence of bulk composition on Ti-Amp, we constructed *T-X* pseudosections with Ti-Amp isopleths, showing mineral assemblages (Fig. 2a) and metamorphic facies (Fig. 2b) at 600–1050 ºC/0.5 GPa, using the compositions applied in Palin et al. (2016). Rock types are arranged to produce general compositional trends from left to right, with a general increase in SiO_2, Al_2O_3, K_2O and Na_2O, and a general decrease in CaO, MgO, FeO and TiO_2. The water-saturated solidus remains almost constant at ~700 ºC. The amphibole-out temperature is around 1020 ºC for different basaltic compositions, but drastically drops down to ~850 ºC for the dioritic composition.

Ti-Amp isopleths are near-flat in the ilmenite-present fields, but show variations up to 60 ºC in the titanite-present fields. Therefore, for the subalkaline rocks, and under the investigated conditions of 0.5 GPa, Ti-Amp shows insignificant dependence on the bulk composition, especially within the ilmenite-present fields.

T-M(TiO_2) pseudosections for MORB composition

The *T-M*(TiO_2) pseudosections are calculated at 0.5 and 1.0 GPa using the MORB composition of Fig. 1, but with varying bulk TiO_2 content (Fig. 3). They show slight variations in the stability boundaries for various minerals. At low pressure (0.5 GPa), ilmenite appears at >750 ºC, while titanite is stable mainly at <750 ºC. At relatively high pressure (1.0 GPa), rutile is stable at >800 ºC while titanite below 800 ºC. If bulk TiO_2 is low enough, Ti-phases disappear.

Both pseudosections, at 0.5 and 1 GPa (Fig. 3a, b), indicate that Ti-Amp isopleths are flat in rutile-present fields, near-flat in ilmenite/titanite-present fields, but exhibit steep negative slopes in Ti-phase-absent fields. Therefore, the dominant control of temperature over Ti-Amp requires the presence of Ti-phases.

DOI: https://doi.org/10.2138/am-2020-7409. http://www.minsocam.org/

T-W(H_2O) pseudosections for MORB composition

The T-W(H_2O) pseudosections are calculated at 0.5 GPa and 1.0 GPa using the MORB composition for Fig. 1, but varying the water content with the rock being near-dry to water-oversaturated (Fig. 4). The solidi are located at 950–1000 ºC under near-dry conditions and at 600–700 ºC under water-saturated conditions. The breakdown of amphibole is controlled by both temperature and the water content. The vertical dashed lines mark the water content used in Fig. 1, which is just saturated at the wet solidus.

The water content has little effect on Ti-Amp for most assemblages, except in the two situations: (i) under subsolidus water-unsaturated conditions, where Ti-Amp tends to increase drastically with decreasing water content; and (ii) with rutile-present assemblages, associated with high water content (>3.5–4 wt%) at high temperature (>850 ºC), which causes a decrease in Ti-Amp.

T-Fe^{3+}/Fe_{total} pseudosections for MORB composition

The effect of fO_2 is shown in the T-Fe^{3+}/Fe_{total} pseudosections at 0.5 and 1.0 GPa for the MORB composition used in Fig. 1, with the Fe^{3+}/Fe_{total} ratio ranging from 0 (all Fe is Fe^{2+}) to 1 (all Fe is Fe^{3+}), and ΔNNO isopleths also shown (Fig. 5). The stability fields of various minerals change with Fe^{3+}/Fe_{total}. Under high Fe^{3+}/Fe_{total} or high fO_2 conditions, the stability fields of ilmenite/hematite gradually extend to the entire temperature range of 600–1050 ºC.

The influence of fO_2 on Ti-Amp is dramatic. For ΔNNO ≤ 2, its influence on the calculated Ti-Amp temperature remains within 40 ºC; but for higher fO_2 or higher Fe^{3+}/Fe_{total} ratios, its influence escalates abruptly.

DOI: https://doi.org/10.2138/am-2020-7409. http://www.minsocam.org/

A new Ti-Amp thermometer

Theoretical background

Hawthorne et al. (2012) proposed a new classification and nomenclature scheme for amphibole. Here are the most concerning issues regarding the occupation of Ti and the definition of calcium amphibole. The general chemical formula of amphibole is $AB_2C_5T_8O_{22}W_2$, where Ti occupies C or T sites. C sites involve 2 *M*(1), 2 *M*(2) and 1 *M*(3) sites. Generally, Ti prefers *M*(1) sites by the reaction ${}^{M(1)}\mathrm{Ti} + 2{}^{\mathrm{W}}\mathrm{O}^{2-} \rightarrow {}^{M(1)}(\mathrm{Mg}, \mathrm{Fe}^{2+}) + 2{}^{\mathrm{W}}(\mathrm{OH}^-)$. Calcium amphibole meets these criteria: (OH, F, Cl) is dominant at W (or alternatively Ti < 0.5); ${}^{B}(\mathrm{Ca} + \sum \mathrm{M}^{2+}) / \sum \mathrm{B} \geq 0.75$, and ${}^{B}\mathrm{Ca} / \sum \mathrm{B} \geq {}^{B}\sum \mathrm{M}^{2+} \geq \sum \mathrm{B}$, where ${}^{B}\sum \mathrm{M}^{2+} = {}^{B}\mathrm{Mg} + {}^{B}\mathrm{Fe}^{2+} + {}^{B}\mathrm{Mn}^{2+}$ and $\sum \mathrm{B} = {}^{B}\mathrm{Li} + {}^{B}\mathrm{Na} + {}^{B}\sum \mathrm{M}^{2+} + {}^{B}\mathrm{Ca} = 2$.

Due to the complex substitutions in amphibole, we consider a simplified model for the distribution of Ti between calcium amphibole and Ti-phases. The thermodynamic background of the Ti-Amp thermometer is shown in a simple reaction

$$\mathrm{TiO_2}^{\mathrm{Ti-phase}} \rightleftharpoons \mathrm{TiO_2}^{\mathrm{Amp}} \quad (1)$$

for which the equilibrium constant is

$$k = \frac{a_{\mathrm{TiO_2}}^{\mathrm{Amp}}}{a_{\mathrm{TiO_2}}^{\mathrm{Ti-phase}}} = \exp\left[\frac{-\Delta G^0}{RT(\mathrm{K})}\right] \quad (2)$$

where $a_{\mathrm{TiO_2}}$ is the activity of TiO_2 in amphibole or Ti-phases, ΔG^0 is the free energy change for Eq. 1 when 'reactants' and 'products' are in their standard states, *R* is the gas constant, and *T*(K) is absolute temperature. Therefore

$$a_{\mathrm{TiO_2}}^{\mathrm{Amp}} = \gamma_{\mathrm{TiO_2}}^{\mathrm{Amp}} X_{\mathrm{TiO_2}}^{\mathrm{Amp}} = a_{\mathrm{TiO_2}}^{\mathrm{Ti-phase}} \exp\left[\frac{-\Delta G^0}{RT(\mathrm{K})}\right] \quad (3)$$

where γ is the activity coefficient, and *X* is the mole fraction. Ti is preferentially accommodated at *M*(1) site, so

$$X_{\mathrm{TiO_2}}^{\mathrm{Amp}} = \mathrm{Ti}^{\mathrm{Amp}}/2 \quad (4)$$

where Ti is in atom per formula unit (apfu). Therefore, Eq. 3 can be rearranged as

$$T(°\mathrm{C}) = \frac{A}{B - \log \mathrm{Ti}^{\mathrm{Amp}}} - 273 \quad (5)$$

where $A = \Delta G^0 \log \mathrm{e}/R$, $B = \log a_{\mathrm{TiO_2}}^{\mathrm{Ti-phase}} - \log \gamma_{\mathrm{TiO_2}}^{\mathrm{Amp}} + \log 2$, and log is the logarithm to base 10.

We intentionally ignore several factors such as the types and compositions of Ti-phases and the variation of $\gamma_{\mathrm{TiO_2}}^{\mathrm{Amp}}$. Based on the simplification, *A* and *B* are constants in Eq. 5.

Method and results

The experimental dataset (DS) is built with 220 crystallization and melting experiments from past publications (Caricchi et al., 2006; Carroll and Wyllie, 1989; Ernst and Liu, 1998; Gardien et al., 2000; Helz, 1973; Holtz et al., 2005; Koepke et al., 2003; Nekvasil et al., 2004; Patiño Douce and Beard, 1995; Pietranik et al., 2009; Pilet et al., 2010; Prouteau and Scaillet, 2003; Rapp and Watson, 1995; Scaillet and Evans, 1999; Scoates et al., 2006; Skjerlie and Johnston, 1996). These researches performed at least one experiment with amphibole + Ti-phase products. Considering that the equilibrium involving Ti might be difficult to achieve due to the likely low diffusion rates in pre-existing Ti-rich mafic minerals (amphibole/biotite), melting experiments are classified into two types according to whether amphibole/biotite is absent (type I) or present (type II) in their starting materials. Oxygen fugacity is converted to absolute fO_2 values and ΔNNO based on Ulmer and Luth (1991) (for graphite-COH buffer) and Frost (1991) (for other buffers). The amphibole formulae are calculated following Ridolfi et al. (2018), but the results are similar with other calculation procedures (e.g. Hawthorne et al., 2012; Holland and Blundy, 1994) except Fe^{3+}/Fe ratios.

Both the pseudosections for calcium amphibole (Figs. 1-5) and previous researches (Ernst and Liu, 1998; Helz, 1973; Molina et al., 2009) reveal that Ti-Amp is mainly influenced by the factors involving temperature, fO_2, bulk composition, water content, and the presence of Ti-phases. Therefore, experiments for calibrating this Ti-Amp thermometer are selected based on the following rules:

(1) Amphibole products in the experiment are calcium amphibole of (OH, F, Cl)-dominant group;

(2) Subalkaline systems;

(3) fO_2 is no more than 2 log units above the Ni-NiO redox buffer (ΔNNO $\leq$ 2);

(4) Ti-phases (rutile, ilmenite or titanite) are present;

The water content is not included in the criteria, because there are no experiments that were performed under the subsolidus water-unsaturated conditions, or that had rutile products with $T >$ 850 ºC and H_2O > 3.5 wt%.

Using these criteria, 93 experiments are selected, including 59 crystallization, 13 type-I melting and 21 type-II melting experiments. The amphibole products have Ti = 0.09–0.49 apfu, Si = 6.0–7.3 apfu, Ca=1.2 – 2.0 apfu, and Mg# = 0.4–0.7. Thirty-six of them are magnesio-hornblende, 26 are pargasite, 27 are sadanagaite, and 4 are tschermakite (Fig. 6a).

According to the Ti-Amp *vs*. temperature diagram (Fig. 6b), the crystallization and type-I melting experiments show a good trend, but the type-II melting experiments are mostly away from the trend. Thus, the calibration dataset (DSc, n = 72) is built with these crystallization and type-I melting experiments. We use OriginPro 2019 to perform non-linear fitting on DSc adopting the Levenberg Marquardt algorithm (Press et al., 2007) with Ti-Amp as the independent variable and T(ºC) as the dependent variable based on Eq. 5. The calibrated equation is

$$T(°\mathrm{C}) = \frac{2400 \pm 123}{(1.52 \pm 0.11) - \log \mathrm{Ti}^{\mathrm{Amp}}} - 273 \quad (6)$$

with $R^2 = 0.84$, residuals ranging from -63 to 72 ºC, and the standard error (1σ) of ±35 ºC for DSc. The recommended Ti-Amp range is 0.1–0.5 apfu based on the experimental data of DSc, although the results for lower or higher Ti-Amp are anyhow indicative.

Effective factors on Ti-Amp

Residual diagrams are plotted for varying pressure, Ti-phases, water content, fO_2, bulk composition and amphibole subgroup for the crystallization and type-I melting experiments (Fig. 7). No significant correlations are observed between residuals and the concerning factors including Ti-Amp, pressure, fO_2 and the type of Ti-phases for DSc. According to Fig. 7b, d, the presence of Ti-phases and the limitation on fO_2 (ΔNNO ≤ 2) are important to ensure the reliability of the Ti-Amp thermometer, as indicated by Figs. 3, 5. The effect of the water content on Ti-Amp under ilmenite-present conditions is insignificant (Fig. 7c); but in rutile/titanite-present cases, the effect is not fully revealed because the highest water content for the rutile/titanite-present experiments is only ~4 wt%. Fig. 7e is in accordance with the view of Molina et al. (2009) that the affinity of Ti in calcium amphibole may increase in subalkaline trachytoid and alkaline systems, indicating that the Ti-Amp thermometer ought to be applied only to subalkaline systems. Fig. 7f indicates that applying the Ti-Amp thermometer to non-calcium amphibole may lead to poor temperature estimates.

Application of the Ti-Amp thermometer to natural rocks

Igneous rocks

As an example of volcanic rocks, Holocene dacites from Volcán San Pedro contain ~29 wt% of crystals of plagioclase, amphibole, biotite, clinopyroxene, orthopyroxene, titanomagnetite, ilmenite, apatite, zircon, pyrrhotite and chalcopyrite in a matrix of rhyolitic glass, having pre-eruption conditions of T = ~850 ºC, ΔNNO = ~1.3, calculated with the titanomagnetite-ilmenite pair (Costa et al., 2004). The representative amphibole is classified as pargasite with Ti = 0.254 apfu using the procedures by Ridolfi et al. (2018), yielding the temperature of 862 ºC using the Ti-Amp thermometer Eq. 6, which is well consistent with the original estimate.

Minerals in plutonic rocks crystallize at varying temperatures, therefore the Ti-Amp thermometer may yield values different from those obtained with other thermometric methods. Dioritic cumulate xenoliths (MA52, MA168) from Mt. Pelée pyroclastic deposits comprise plagioclase, clinopyroxene, orthopyroxene, amphibole, titanomagnetite and ilmenite, in which the coexisting titanomagnetite and ilmenite yielded T = 790–900 ºC, ΔNNO = ~1 (Fichaut et al., 1989). Representative amphibole analyses show the Ti content of 0.16–0.2 apfu, which gives the temperature of 763–808 ºC using Eq. 6. This estimate is lower than that from the titanomagnetite-ilmenite pair, likely confirming that amphibole in these plutonic rocks crystallized later than other minerals such as titanomagnetite and ilmenite.

Metamorphic rocks

Mafic granulites are suggested to form at >800 ºC or even >900 ºC (e.g. Freise et al., 2009; Palin et al., 2016; Pilet et al., 2010; Springer and Seck, 1997; Wei and Duan, 2019). Although such high temperature favour diffusion, Ti-Amp may have the potential to retrieve amphibole-forming temperature due to the likely slow diffusion rates of Ti in high-temperature rocks.

Ilmenite-bearing mafic granulites from North Hengshan, China, were estimated to have maximum-temperature conditions of 840–860 ºC (at 0.6–0.8 GPa) using pseudosection modelling (Zhang et al., 2018). The bulk Fe^{3+}/Fe_{total} values are 0.12–0.19, suggesting fO_2 is near

NNO. The matrix calcium amphibole has the Ti content of 0.20–0.27 apfu, giving 810–872 ºC from the Ti-Amp thermometer Eq. 6, consistent with the original modelling estimates.

Two samples of ilmenite-bearing amphibole granulite from Huai'an, China, were proposed to have maximum amphibole-forming temperatures of 1010 ºC (17HT13) and 1000 ºC (16HT22), using pseudosection modelling with Ti-Amp and anorthite-in-plagioclase isopleths (Liao and Wei, 2019). The bulk Fe^{3+}/Fe_{total} value of less than 0.09–0.15 suggest that fO_2 is near or more reducing than NNO, and $FeTiO_3/(FeTiO_3 + Fe_2O_3) > 0.95$ in ilmenite (unpublished data of Liao) indicates ΔNNO < -0.9 (Zhao et al., 1999). The maximum Ti-Amp values in samples 17HT13 and 16HT22 are 0.44 and 0.38 apfu, giving 1006 and 964 ºC from the thermometer Eq. 6, respectively. A few amphibole grains show core-rim Ti-decreasing zoning, reflecting the cooling process. These calculations are comparable to the original estimates.

The Ti-Amp thermometer can also give geologically meaningful results for amphibolites. Ilmenite/titanite-bearing amphibolites from north-eastern Taiwan, China, were reported to contain green/blue-green amphibole and brown amphibole, indicating amphibolite-facies metamorphism at 550–700 ºC / ~0.5 GPa and thermal metamorphism at 670–800 ºC / 0.5 GPa / QFM, respectively (Liou et al., 1981). The green and blue-green amphibole has the Ti content of <0.06–0.07 apfu, giving the temperature of 602–624 ºC; while the brown amphibole has higher Ti content of ~0.10–0.22 apfu, yielding the temperature of 679–829 ºC from the thermometer Eq. 6. Both estimates fit well with the original ones.

Discussion

Comparison of Ti-Amp isopleths and thermometer

Comparing the results of Ti-Amp isopleths in pseudosections and the Ti-Amp thermometer Eq. 6, the differences in temperature estimates are within 90 ºC for the MORB composition in

DOI: https://doi.org/10.2138/am-2020-7409. http://www.minsocam.org/

Fig. 1, and within 30 and 50 ºC for the two samples of Liao and Wei (2019). Such differences are likely caused by the compositional effect (Figs. 2, 4, 5) because pseudosection modelling is performed for specific bulk compositions.

Comparing the two methods, pseudosection modelling with Ti-Amp isopleths not only gives information on amphibole-forming temperature, but comprehensively considers the stability and compositions of amphibole and other minerals, to construct *P*-*T* paths or evaluate the reliability of the *P*-*T* results; while the Ti-Amp thermometer is quick and easy to apply. However, uncertainties exist in both methods, and more research is required to improve their accuracy.

Comparison with other amphibole-only thermometers

There have been a few thermometers that consider the composition of amphibole exclusively. As for Ti-Amp thermometers, Otten (1984) calibrated one based on a limited number of experiments, and Ernst and Liu (1998) proposed a semi-quantitative Ti-in-calcic-amphibole thermometer, whose ideas have been adopted and further developed in this study. As for amphibole-only multi-component thermometers, Ridolfi and Renzulli (2012) proposed one improved from that of Ridolfi et al. (2010), involving nearly all major cations in amphibole as well as pressure; and Putirka (2016) proposed formulae involving the chemical components of Si, Ti, Na, Fe/Mg with or without the effect of pressure. Therefore, we compare the results of our thermometer and the formulae of Otten (1984), Ridolfi and Renzulli (2012) and Putirka (2016), for the crystallization and type-I melting experiments (Fig. 8).

As for the experiments under the aforementioned applicable conditions for the Ti-Amp thermometer (DSc), our new Ti-Amp thermometer shows better results than the antecedent one of Otten (1984), especially at the calculated temperatures of ~800 ºC. The multi-component thermometers of Ridolfi and Renzulli (2012) and Putirka (2016) do not provide better results

DOI: https://doi.org/10.2138/am-2020-7409. http://www.minsocam.org/

than the Ti-Amp thermometers for DSc. However, for the experiments under other conditions (e.g. Ti-phases absent, in alkaline systems), the multi-component thermometers yield better fitting than the Ti-Amp thermometers. These observations suggest that our updated Ti-Amp thermometer is particularly suitable for its applicable conditions (in subalkaline systems, ΔNNO ≤ 2, with the presence of Ti-phases), and also resistant to cation diffusion during slow cooling; while the multi-component thermometers can be applied to wider conditions, although their application to high-grade metamorphic rocks, which mostly involve long-duration post-peak cooling, needs further testing.

Amphibole composition and metamorphic grade

Raase (1974) pointed out that higher Ti content of amphibole can be linked to higher metamorphic grades. Albeit we have obtained quantitative relations between Ti-Amp and temperature, it is beneficial to improve the relation between Ti-Amp and metamorphic grade of Raase (1974), simply by splitting the granulite facies into the HT granulite facies ($T \leq 900$ ºC) and the UHT granulite facies (> 900 ºC). We add a few recent research data of natural amphibole (Ernst, 1988; Liao and Wei, 2019; Liou et al., 1981; Prakash et al., 2007; Prakash et al., 2010; Qian and Wei, 2016; Zhang et al., 2018) to the original figure 2 of Raase (1974) to obtain Fig. 9. The upper and lower limits of Ti-Amp are used as the compositional analyses when only Ti-Amp ranges are known. In addition, we also plot the correlative temperatures from the new Ti-Amp thermometer along the vertical axis on the right side of the diagram. Statistically, higher Ti-Amp indicates higher metamorphic grade. Some data points (several bars plotted separately in the histogram) with extremely high Ti-Amp values for its metamorphic facies are suspicious, while some with very low Ti-Amp may result from the Ti-unsaturation (Raase, 1974).

With increasing temperature, the Si content of amphibole (Si-Amp) tends to decrease due to tschermak substitution (Kostyuk and Sobolev, 1969), therefore Si-Amp and Ti-Amp may jointly represent metamorphic facies if Ti-phases are present. Hence we plot the Si *vs.* Ti in amphibole diagram using the experiments in DSc (Fig. 10). Based on Wei and Duan (2019) and Fig. 1b, the correlative metamorphic facies are defined by experimental temperature: the high amphibolite facies for 680–800 ºC, the HT granulite facies for 800–900 ºC, and the UHT granulite facies for >900 ºC. Consistent with the theoretical analysis, higher-temperature amphibole tends to be Ti-richer and Si-poorer. Applying Fig. 10 to the data of natural amphibole reported in past publications, such as amphibolites from Wutai, China (Qian and Wei, 2016), HT granulites from northern Hengshan, China (Zhang et al., 2018), UHT granulites from Huai'an, China (Liao and Wei, 2019), and UHT granulites from the Madurai Block, southern India (Prakash et al., 2010), we found that all the results are consistent. Accordingly, the Si *vs.* Ti in amphibole diagram (Fig. 10) is an easy way to roughly express metamorphic facies for the rocks that contain amphibole coexisting with Ti-phases.

Implications

Ti-Amp is powerful in retrieving calcium-amphibole-forming temperature in subalkaline systems when amphibole is in equilibrium with Ti-phases at $\Delta NNO \leq 2$, according to pseudosection modelling and experimental data. The Ti-Amp thermometer (Eq. 6) has been calibrated to simply recover calcium-amphibole-forming temperature for natural igneous and high-grade metamorphic rocks. Moreover, we have discussed the relations between Ti-Amp and metamorphic facies, and introduced the Si *vs.* Ti in amphibole diagram as a simple tool to indicate metamorphic facies.

The differences between the results of the Ti-Amp thermometer and the isopleths in pseudosections may partly stem from the consideration of bulk composition and fO_2. Pseudosection modelling provides detailed information regarding the metamorphic evolution of studied rocks, hence the temperatures defined in pseudosections are easily connected to certain evolutionary stages. In contrast, the Ti-Amp thermometer is easy and quick to be applied to natural rocks that contain calcium amphibole and Ti-phases.

However, further research is considerably needed on amphibole-related subjects. More high-quality experiments for low-mobility components such as Ti are needed to attain better knowledge of the crystalline and thermodynamic property of amphibole, and the interaction between amphibole and other phases. Such work will significantly contribute to calibrating both conventional thermometers and thermodynamic models.

To obtain reliable results, the Ti-Amp thermometer (Eq. 6) should be strictly applied to the conditions recommended in this contribution. Only calcium amphibole in subalkaline systems should be selected for temperature calculation with the formula. The fO_2 values may be difficult to obtain in some cases, but at least a rough estimate is necessary to ensure ΔNNO ≤ 2. Moreover, this thermometer may underestimate temperature in high-temperature (>850 ºC) rutile-present cases with significant water content (> 3.5–4 wt%), and overestimate temperature for amphibole associated with subsolidus water-unsaturated conditions, which can be evidenced by the existence of some non-equilibrium textures or low water content (<1–1.5 wt%). In addition, for amphibole with exsolution of Ti-phases (Mongkoltip and Ashworth, 1983; Otten, 1984), it is necessary to recover pre-exsolution compositions before performing the calculation.

Acknowledgements

This work is financially supported by the National Natural Science Foundation of China (Grant Numbers 41872057, 41430207). We are grateful to Prof. Johann Diener for technical help. We appreciate constructive reviews by Prof. Richard Palin and all the anonymous reviewers, and the meticulous editorial assistance by Dr Antonio Acosta-Vigil.

References cited

Bard, J.P. (1970) Composition of hornblendes formed during the hercynian progressive metamorphism of the Aracena metamorphic belt (SW Spain). Contributions to Mineralogy and Petrology, 28(2), 117-134.

Blundy, J., and Cashman, K. (2008) Petrologic reconstruction of magmatic system variables and processes. Reviews in Mineralogy and Geochemistry, 69, 179-239.

Caricchi, L., Ulmer, P., and Peccerillo, A. (2006) A high-pressure experimental study on the evolution of the silicic magmatism of the Main Ethiopian Rift. Lithos, 91(1-4), 46-58.

Carroll, M.R., and Wyllie, P.J. (1989) Experimental phase-relations in the system tonalite-peridotite-H_2O at 15 Kb - Implications for assimilation and differentiation processes near the crust-mantle boundary. Journal of Petrology, 30(6), 1351-1382.

Costa, F., Scaillet, B., and Pichavant, M. (2004) Petrological and experimental constraints on the pre-eruption compositions of Holocene dacite from Volcán San Pedro (36°S, Chilean Andes) and importance of sulphur in silicic subduction-related magmas. Journal of Petrology, 45(4), 855-881.

Ernst, W.G. (1988) Element partitioning and thermobarometry in polymetamorphic late Archean and Early-Mid Proterozoic rocks from eastern Liaoning and southern Jilin provinces, China. American Journal of Science, 288, 293-340.

Ernst, W.G., and Liu, J. (1998) Experimental phase-equilibrium study of Al- and Ti-contents of calcic amphibole in MORB—A semiquantitative thermobarometer. American Mineralogist, 83(9-10), 952-969.

Fichaut, M., Marcelot, G., and Clocchiatti, R. (1989) Magmatology of Mt. Pelée (Martinique, F.W.I.); II, Petrology of gabbroic and dioritic cumulates. Journal of Volcanology and Geothermal Research, 38(1-2), 171-187.

Freise, M., Holtz, F., Nowak, M., Scoates, J.S., and Strauss, H. (2009) Differentiation and crystallization conditions of basalts from the Kerguelen large igneous province: An experimental study. Contributions to Mineralogy and Petrology, 158(4), 505-527.

Frost, B.R. (1991) Introduction to oxygen fugacity and its petrologic importance. Reviews in Mineralogy and Geochemistry, 25(1), 1-9.

Frost, B.R., and Chacko, T. (1989) The granulite uncertainty principle: Limitations on thermobarometry in granulites. Journal of Geology, 97(4), 435-450.

Gardien, V., Thompson, A.B., and Ulmer, P. (2000) Melting of biotite plus plagioclase plus quartz gneisses: the role of H_2O in the stability of amphibole. Journal of Petrology, 41(5), 651-666.

Green, E.C.R., White, R.W., Diener, J.F.A., Powell, R., Holland, T.J.B., and Palin, R.M. (2016) Activity-composition relations for the calculation of partial melting equilibria in metabasic rocks. Journal of Metamorphic Geology, 34(9), 845-869.

Harley, S.L. (1989) The origins of granulites: A metamorphic perspective. Geological Magazine, 126(3), 215-247.

Harley, S.L. (1998) On the occurrence and characterization of ultrahigh-temperature crustal metamorphism. Geological Society, London, Special Publications, 138(1), 81-107.

Hawthorne, F.C., Oberti, R., Harlow, G.E., Maresch, W.V., Martin, R.F., Schumacher, J.C., and Welch, M.D. (2012) Nomenclature of the amphibole supergroup. American Mineralogist, 97(11-12), 2031-2048.

Helz, R.T. (1973) Phase relations of basalts in their melting range at PH_2O = 5 kb as a function of oxygen fugacity: Part I. Mafic phases. Journal of Petrology, 14(2), 249-302.

Holland, T., and Blundy, J. (1994) Non-ideal interactions in calcic amphiboles and their bearing on amphibole-plagioclase thermometry. Contributions to Mineralogy and Petrology, 116(4), 433-447.

Holland, T., and Powell, R. (2003) Activity-composition relations for phases in petrological calculations: An asymmetric multicomponent formulation. Contributions to Mineralogy and Petrology, 145(4), 492-501.

Holland, T.J.B., and Powell, R. (2011) An improved and extended internally consistent thermodynamic dataset for phases of petrological interest, involving a new equation of state for solids. Journal of Metamorphic Geology, 29(3), 333-383.

Holtz, F., Sato, H., Lewis, J., Behrens, H., and Nakada, S. (2005) Experimental petrology of the 1991-1995 Unzen dacite, Japan. Part I: Phase relations, phase composition and pre-eruptive conditions. Journal of Petrology, 46(2), 319-337.

Koepke, J., Berndt, J., and Bussy, F. (2003) An experimental study on the shallow-level migmatization of ferrogabbros from the Fuerteventura Basal Complex, Canary Islands. Lithos, 69(3-4), 105-125.

Koester, E., Pawley, A.R., Fernandes, L.A.D., Porcher, C.C., and Soliani, E. (2002) Experimental melting of cordierite gneiss and the petrogenesis of syntranscurrent peraluminous granites in southern Brazil. Journal of Petrology, 43(8), 1595-1616.

Kostyuk, E.A., and Sobolev, V.S. (1969) Paragenetic types of calciferous amphiboles of metamorphic rocks. Lithos, 2(1), 67-81.

Li, X.W., and Wei, C.J. (2016) Phase equilibria modelling and zircon age dating of pelitic granulites in Zhaojiayao, from the Jining Group of the Khondalite Belt, North China Craton. Journal of Metamorphic Geology, 34(6), 595-615.

Liao, Y., and Wei, C.J. (2019) Ultrahigh-temperature mafic granulite in the Huai'an Complex, North China Craton: Evidence from phase equilibria modelling and amphibole thermometers. Gondwana Research, 76, 62-76.

Liou, J.G., Ernst, W.G., and Moore, D.E. (1981) Geology and petrology of some polymetamorphosed amphibolites and associated rocks in northeastern Taiwan: Summary. Geological Society of America Bulletin, 92(5), 219-224.

Liu, T., and Wei, C.J. (2018) Metamorphic evolution of Archean ultrahigh-temperature mafic granulites from the western margin of Qian’an gneiss dome, eastern Hebei Province, North China Craton: Insights into the Archean tectonic regime. Precambrian Research, 318, 170-187.

Molina, J.F., Scarrow, J.H., Montero, P.G., and Bea, F. (2009) High-Ti amphibole as a petrogenetic indicator of magma chemistry: evidence for mildly alkalic-hybrid melts during evolution of Variscan basic-ultrabasic magmatism of Central Iberia. Contributions to Mineralogy and Petrology, 158(1), 69-98.

Molina, J.F., Moreno, J.A., Castro, A., Rodriguez, C., and Fershtater, G.B. (2015) Calcic amphibole thermobarometry in metamorphic and igneous rocks: New calibrations based on plagioclase/amphibole Al-Si partitioning and amphibole/liquid Mg partitioning. Lithos, 232, 286-305.

Mongkoltip, P., and Ashworth, J.R. (1983) Exsolution of ilmenite and rutile in hornblende. American Mineralogist, 68(1-2), 143-155.

DOI: https://doi.org/10.2138/am-2020-7409. http://www.minsocam.org/

Nekvasil, H., Dondolini, A., Horn, J., Filiberto, J., Long, H., and Lindsley, D.H. (2004) The origin and evolution of silica-saturated alkalic suites: an experimental study. Journal of Petrology, 45(4), 693-721.

Otten, M.T. (1984) The origin of brown hornblende in the Artfjället gabbro and dolerites. Contributions to Mineralogy and Petrology, 86(2), 189-199.

Palin, R.M., White, R.W., Green, E.C.R., Diener, J.F.A., Powell, R., and Holland, T.J.B. (2016) High-grade metamorphism and partial melting of basic and intermediate rocks. Journal of Metamorphic Geology, 34(9), 871-892.

Patiño Douce, A.E., and Beard, J.S. (1995) Dehydration-melting of biotite gneiss and quartz amphibolite from 3 to 15 Kbar. Journal of Petrology, 36(3), 707-738.

Pattison, D.R.M., Chacko, T., Farquhar, J., and McFarlane, C.R.M. (2003) Temperatures of granulite-facies metamorphism: Constraints from experimental phase equilibria and thermobarometry corrected for retrograde exchange. Journal of Petrology, 44(5), 867-900.

Pietranik, A., Holtz, F., Koepke, J., and Puziewicz, J. (2009) Crystallization of quartz dioritic magmas at 2 and 1 kbar: Experimental results. Mineralogy and Petrology, 97(1-2), 1-21.

Pilet, S., Ulmer, P., and Villiger, S. (2010) Liquid line of descent of a basanitic liquid at 1.5 GPa: Constraints on the formation of metasomatic veins. Contributions to Mineralogy and Petrology, 159(5), 621-643.

Powell, R., Holland, T., and Worley, B. (1998) Calculating phase diagrams involving solid solutions via non-linear equations, with examples using THERMOCALC. Journal of Metamorphic Geology, 16(4), 577-588.

Prakash, D., Arima, M., and Mohan, A. (2007) Ultrahigh-temperature mafic granulites from Panrimalai, south India: Constraints from phase equilibria and thermobarometry. Journal of Asian Earth Sciences, 29(1), 41-61.

Prakash, D., Prakash, S., and Sachan, H.K. (2010) Petrological evolution of the high pressure and ultrahigh-temperature mafic granulites from Karur, southern India: evidence for decompressive and cooling retrograde trajectories. Mineralogy and Petrology, 100(1-2), 35-53.

Press, W.H., Teukolsky, S.A., Vetterling, W.T., and Flannery, B.P. (2007) Nonlinear Models. Numerical Recipes in C. Cambridge University Press.

Prouteau, G., and Scaillet, B. (2003) Experimental constraints on the origin of the 1991 Pinatubo dacite. Journal of Petrology, 44(12), 2203-2241.

Putirka, K. (2016) Amphibole thermometers and barometers for igneous systems and implications for eruption mechanisms of felsic magmas at arc volcanoes. American Mineralogist, 101(3-4), 841-858.

Qian, J.H., and Wei, C.J. (2016) *P-T-t* evolution of garnet amphibolites in the Wutai-Hengshan area, North China Craton: Insights from phase equilibria and geochronology. Journal of Metamorphic Geology, 34(5), 423-446.

Raase, P. (1974) Al and Ti contents of hornblende, indicators of pressure and temperature of regional metamorphism. Contributions to Mineralogy and Petrology, 45(3), 231-236.

Rapp, R.P., and Watson, E.B. (1995) Dehydration melting of metabasalt at 8–32 kbar: Implications for continental growth and crust-mantle recycling. Journal of Petrology, 36(4), 891-931.

DOI: https://doi.org/10.2138/am-2020-7409. http://www.minsocam.org/

Ridolfi, F., and Renzulli, A. (2012) Calcic amphiboles in calc-alkaline and alkaline magmas: Thermobarometric and chemometric empirical equations valid up to 1,130 °C and 2.2 GPa. Contributions to Mineralogy and Petrology, 163(5), 877-895.

Ridolfi, F., Renzulli, A., and Puerini, M. (2010) Stability and chemical equilibrium of amphibole in calc-alkaline magmas: an overview, new thermobarometric formulations and application to subduction-related volcanoes. Contributions to Mineralogy and Petrology, 160(1), 45-66.

Ridolfi, F., Zanetti, A., Renzulli, A., Perugini, D., Holtz, F., and Oberti, R. (2018) AMFORM, a new mass-based model for the calculation of the unit formula of amphiboles from electron microprobe analyses. American Mineralogist, 103(7), 1112-1125.

Rushmer, T. (1993) Experimental high-pressure granulites: Some applications to natural mafic xenolith suites and Archean granulite terranes. Geology, 21(5), 411-414.

Santosh, M., Tsunogae, T., Li, J.H., and Liu, S.J. (2007) Discovery of sapphirine-bearing Mg-Al granulites in the North China Craton: Implications for paleoproterozoic ultrahigh temperature metamorphism. Gondwana Research, 11(3), 263-285.

Scaillet, B., and Evans, B.W. (1999) The 15 June 1991 eruption of Mount Pinatubo. I. Phase equilibria and pre-eruption P-T-fO_2-fH_2O conditions of the dacite magma. Journal of Petrology, 40(3), 381-411.

Scoates, J.S., Lo Cascio, M., Weis, D., and Lindsley, D.H. (2006) Experimental constraints on the origin and evolution of mildly alkalic basalts from the Kerguelen Archipelago, Southeast Indian Ocean. Contributions to Mineralogy and Petrology, 151(5), 582-599.

Sen, C., and Dunn, T. (1994) Dehydration melting of a basaltic composition amphibolite at 1.5 and 2.0 GPa: Implications for the origin of adakites. Contributions to Mineralogy and Petrology, 117(4), 394-409.

DOI: https://doi.org/10.2138/am-2020-7409. http://www.minsocam.org/

Skjerlie, K.P., and Johnston, A.D. (1996) Vapour-absent melting from 10 to 20 kbar of crustal rocks that contain multiple hydrous phases: Implications for anatexis in the deep to very deep continental crust and active continental margins. Journal of Petrology, 37(3), 661-691.

Spear, F.S. (1980) NaSi$\rightleftharpoons$CaAl exchange equilibrium between plagioclase and amphibole. Contributions to Mineralogy and Petrology, 72(1), 33-41.

Spear, F.S. (1981) An experimental-study of hornblende stability and compositional variability in amphibolite. American Journal of Science, 281(6), 697-734.

Spear, F.S., and Florence, F.P. (1992) Thermobarometry in granulites: Pitfalls and new approaches. Precambrian Research, 55(1-4), 209-241.

Springer, W., and Seck, H.A. (1997) Partial fusion of basic granulites at 5 to 15 kbar: Implications for the origin of TTG magmas. Contributions to Mineralogy and Petrology, 127(1-2), 30-45.

Ulmer, P., and Luth, R.W. (1991) The graphite-COH fluid equilibrium in P, T, fO_2 space. Contributions to Mineralogy and Petrology, 106(3), 265-272.

Wei, C.J., and Duan, Z.Z. (2019) Phase relations in metabasic rocks: constraints from the results of experiments, phase modelling and ACF analysis. Geological Society, London, Special Publications, 474(1), 25-45.

White, R.W., Powell, R., Holland, T.J.B., and Worley, B.A. (2000) The effect of TiO_2 and Fe_2O_3 on metapelitic assemblages at greenschist and amphibolite facies conditions: Mineral equilibria calculations in the system K_2O-FeO-MgO-Al_2O_3-SiO_2-H_2O-TiO_2-Fe_2O_3. Journal of Metamorphic Geology, 18(5), 497-511.

White, R.W., Powell, R., Holland, T.J.B., Johnson, T.E., and Green, E.C.R. (2014) New mineral activity-composition relations for thermodynamic calculations in metapelitic systems. Journal of Metamorphic Geology, 32(3), 261-286.

Whitney, D.L., and Evans, B.W. (2010) Abbreviations for names of rock-forming minerals. American Mineralogist, 95(1), 185-187.

Wyllie, P.J., and Wolf, M.B. (1993) Amphibolite dehydration-melting: Sorting out the solidus. Geological Society, London, Special Publications, 76(1), 405-416.

Yang, C., and Wei, C.J. (2017) Ultrahigh temperature (UHT) mafic granulites in the East Hebei, North China Craton: Constraints from a comparison between temperatures derived from REE-based thermometers and major element-based thermometers. Gondwana Research, 46, 156-169.

Zhang, Y.H., Wei, C.J., Lu, M.J., and Zhou, X.W. (2018) *P-T-t* evolution of the high-pressure mafic granulites from northern Hengshan, North China Craton: Insights from phase equilibria and geochronology. Precambrian Research, 312, 1-15.

Zhao, D., Essene, E.J., and Zhang, Y. (1999) An oxygen barometer for rutile–ilmenite assemblages: oxidation state of metasomatic agents in the mantle. Earth and Planetary Science Letters, 166(3-4), 127-137.

Figures

Fig. 1. *P*-*T* pseudosections for the MORB composition used in Palin et al. (2016) with mineral assemblages **(a)** and metamorphic facies **(b)**. Dash-dotted curves are Ti-in-amphibole (Ti-Amp) isopleths, labelled with 5–40, representing Ti-Amp of 0.05–0.40 apfu. Solid curves represent the stability boundaries of the selected minerals. Mineral abbreviations are the same as in Whitney and Evans (2010). Metamorphic facies abbreviations: EC, eclogite facies; Grt AM/HP-GR, garnet amphibolite and high-pressure (HP) granulite facies; HAM, high amphibolite facies; HT-GR, high-temperature (HT) granulite facies; LAM, low amphibolite facies; UHT, ultrahigh-temperature granulite facies. Mineral assemblages labelled with digits in panel a are shown at the right side.

Fig. 2. *T*-*X* pseudosections calculated at 0.5 GPa, showing the variations of Ti-Amp with phase assemblage **(a)** and metamorphic facies **(b)** in transition between different lithologies. Rock types are arranged to produce the general compositional trends from left to right, constituting a general increase in SiO_2, Al_2O_3, K_2O and Na_2O, and a general decrease in CaO, MgO, FeO and TiO_2. The compositions of these rocks are the same as in Palin et al. (2016) and marked as vertical dashed lines. Other details are the same as in Fig. 1.

Fig. 3. *T*-*M*(TiO_2) pseudosections for the MORB composition at 0.5 GPa **(a)** and 1 GPa **(b)**. Vertical dashed lines represent the TiO_2 content used in Fig. 1. Other details are the same as in Fig. 1.

DOI: https://doi.org/10.2138/am-2020-7409. http://www.minsocam.org/

Fig. 4. *T*-*W*(H_2O) pseudosections for the MORB composition at 0.5 GPa **(a)** and 1 GPa **(b)**. Vertical dashed lines represent the water content used in Fig. 1. Other details are the same as in Fig. 1.

Fig. 5. *T*-Fe^{3+}/Fe_{total} pseudosections for the MORB composition used in Fig. 1 with ΔNNO isopleths at 0.5 GPa **(a)** and 1 GPa **(b)**. Dotted curves represent ΔNNO isopleths. Vertical dashed lines represent the Fe^{3+}/Fe_{total} value used in Fig. 1. Other details are the same as in Fig. 1.

Fig. 6. (a) The classification of calcium amphibole from the selected experiments based on Hawthorne et al. (2012). **(b)** Ti-Amp *vs. T* diagram with the calibrated thermometer. Data from the crystallization and melting experiments from the previous researches are filtered with the criteria: calcium amphibole of W(OH, F, Cl)-dominant group, $\Delta NNO \leq 2$, Ti-phases present, subalkaline system. Melting experiments are classified according to their starting materials that are amphibole/biotite-absent (type I) or amphibole/biotite-present (type II). The crystallization and type-I melting experiments exhibit a good trend and are included in the calibration dataset (DSc). Non-linear fitting is performed for the thermometer on DSc using OriginPro 2019 with the Levenberg Marquardt algorithm.

Fig. 7. Residual diagrams for the thermometer on pressure **(a)**, Ti-Amp for Ti-phases **(b)**, *W*(H_2O) **(c)**, ΔNNO **(d)**, Ti-Amp for different bulk compositions **(e)**, and Ti-Amp for different amphibole subgroups **(f)**. The experimental data of DSc are included in all the panels. Besides, in

DOI: https://doi.org/10.2138/am-2020-7409. http://www.minsocam.org/

the panels **b, d, e, f**, we add the experiments that meet the criteria for DSc except for those of Ti-phases, fO_2, bulk composition, and amphibole types, respectively. Solid horizontal lines represent residual = 0, and dashed horizontal lines represent residual = ±2σ.

Fig. 8. *T* calculated *vs.* *T* measured diagrams showing the comparison between the calculated results using different amphibole-only thermometers and the measured temperatures in the crystallization and type-I melting experiments in DS. Dashed lines are 1-to-1 lines for *T* calculated *vs.* *T* measured. Slope and intercept values on regression lines (*T* calculated *vs.* *T* measured, not plotted) should ideally be 1.0 and 0, respectively. **(a)** The thermometer Eq. 6 proposed in this study. **(b)** The Ti-Amp thermometer in Otten (1984). **(c)** Eq. 2 in Ridolfi and Renzulli (2012), involving Si, Ti, Al, Fe, Mg, Ca, Na and K in amphibole as well as pressure. **(d)** Eq. 5 in Putirka (2016), involving Si, Ti, Fe and Na in amphibole.

Fig. 9. A histogram showing Ti-Amp in rocks metamorphosed under different metamorphic facies based on Raase (1974) with supplementary natural amphibole data from the literature (Ernst, 1988; Liao and Wei, 2019; Liou et al., 1981; Prakash et al., 2007; Prakash et al., 2010; Qian and Wei, 2016; Zhang et al., 2018). Temperature values shown on the right side along the vertical axis are calculated using the new Ti-Amp thermometer Eq. 6. Ep-AM refers to the epidote-amphibole facies, and other metamorphic facies abbreviations are the same as in Fig. 1.

DOI: https://doi.org/10.2138/am-2020-7409. http://www.minsocam.org/

Fig. 10. A Si *vs.* Ti in amphibole diagram for the experimental data of DSc with the proposed boundaries defining the high amphibolite (HAM), HT granulite (GR) and UHT granulite facies.

DOI: https://doi.org/10.2138/am-2020-7409. http://www.minsocam.org/

Supplementary tables

Supplementary table 1. Crystallization and melting experiments used in this study.

Supplementary table 2. Ti-in-calcium-amphibole thermometer calculator.

Fig. 1

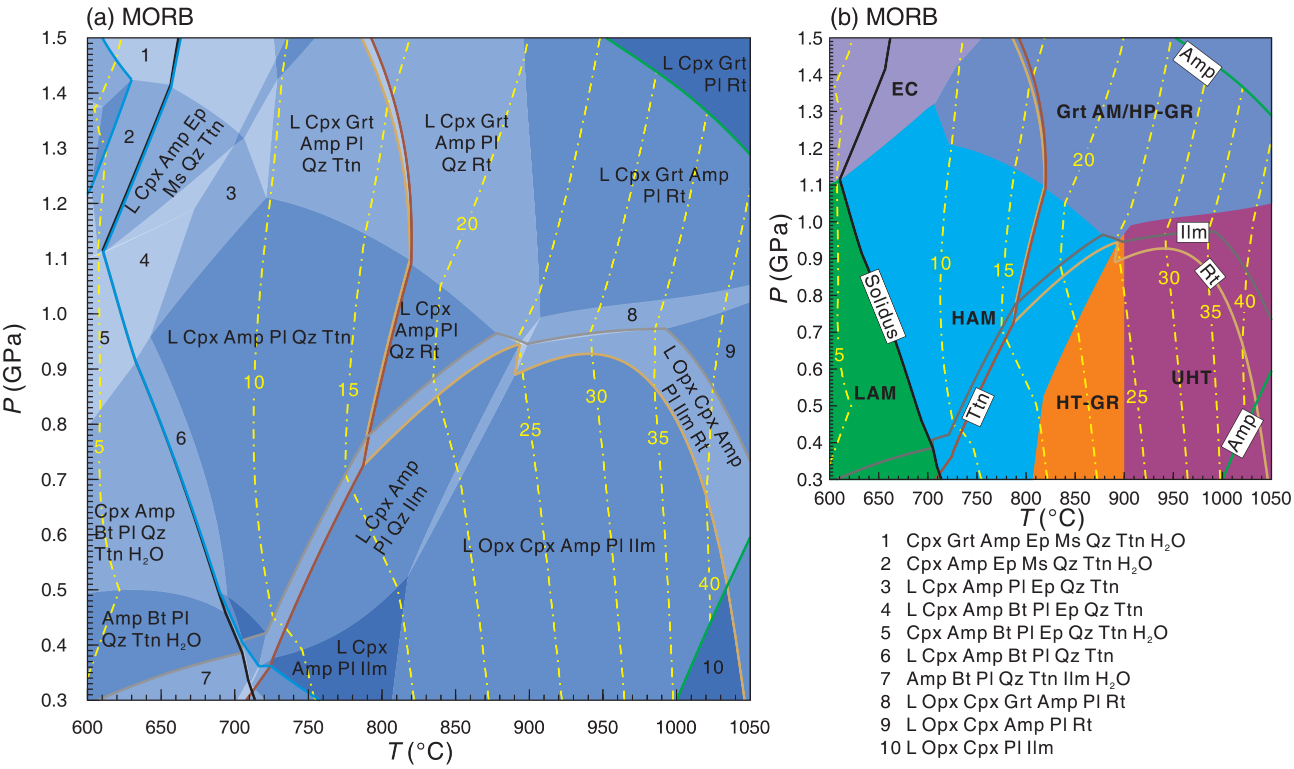

1 Cpx Grt Amp Ep Ms Qz Ttn H_2O
2 Cpx Amp Ep Ms Qz Ttn H_2O
3 L Cpx Amp Pl Ep Qz Ttn
4 L Cpx Amp Bt Pl Ep Qz Ttn
5 Cpx Amp Bt Pl Ep Qz Ttn H_2O
6 L Cpx Amp Bt Pl Qz Ttn
7 Amp Bt Pl Qz Ttn Ilm H_2O
8 L Opx Cpx Grt Amp Pl Rt
9 L Opx Cpx Amp Pl Rt
10 L Opx Cpx Pl Ilm

DOI: https://doi.org/10.2138/am-2020-7409. http://www.minsocam.org/

Fig. 2

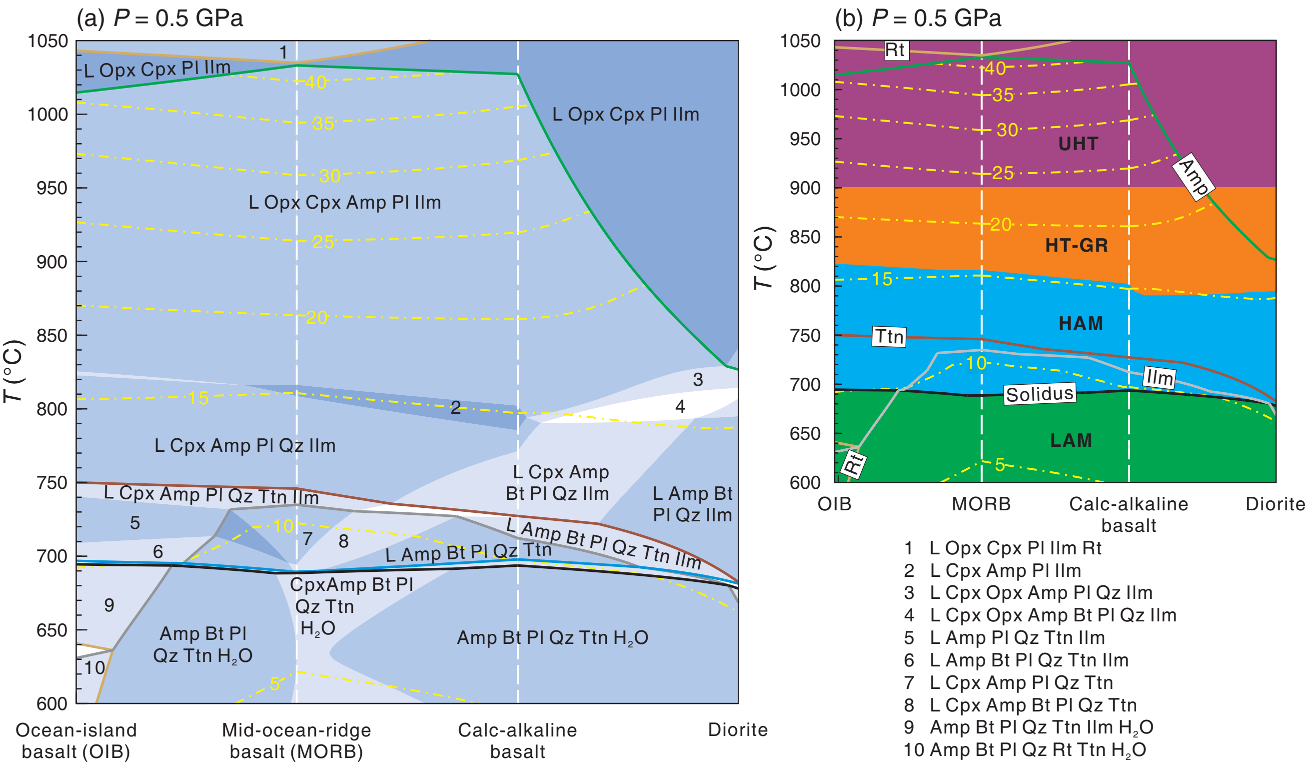

This is the peer-reviewed, final accepted version for American Mineralogist, published by the Mineralogical Society of America.
The published version is subject to change. Cite as Authors (Year) Title. American Mineralogist, in press.
DOI: https://doi.org/10.2138/am-2020-7409. http://www.minsocam.org/

Fig. 3

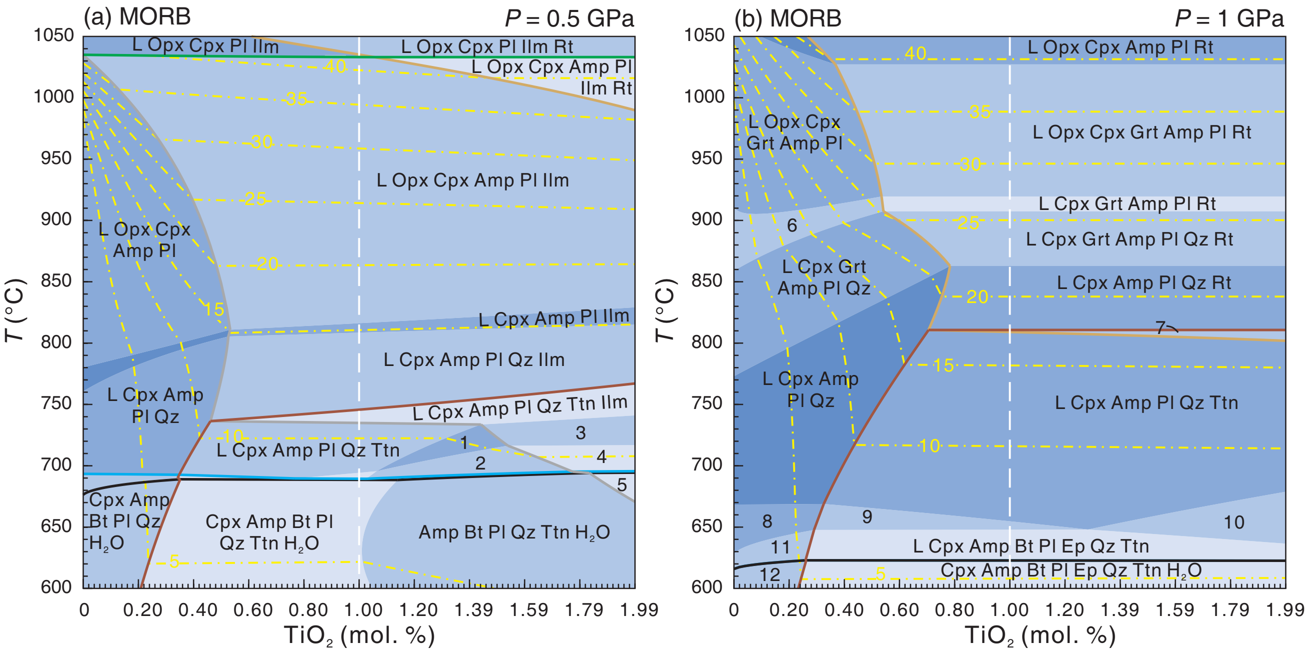

1 L Amp Pl Qz Ttn
2 L Amp Bt Pl Qz Ttn
3 L Amp Pl Qz Ttn Ilm
4 L Amp Bt Pl Qz Ttn Ilm
5 Amp Bt Pl Qz Ttn Ilm H_2O
6 L Cpx Grt Amp Pl
7 L Cpx Amp Pl Qz Ttn Rt
8 L Cpx Amp Pl Ep Qz
9 L Cpx Amp Pl Ep Qz Ttn
10 L Cpx Amp Bt Pl Qz Ttn
11 L Cpx Amp Bt Pl Ep Qz
12 Cpx Amp Bt Pl Ep Qz H_2O

Fig. 4

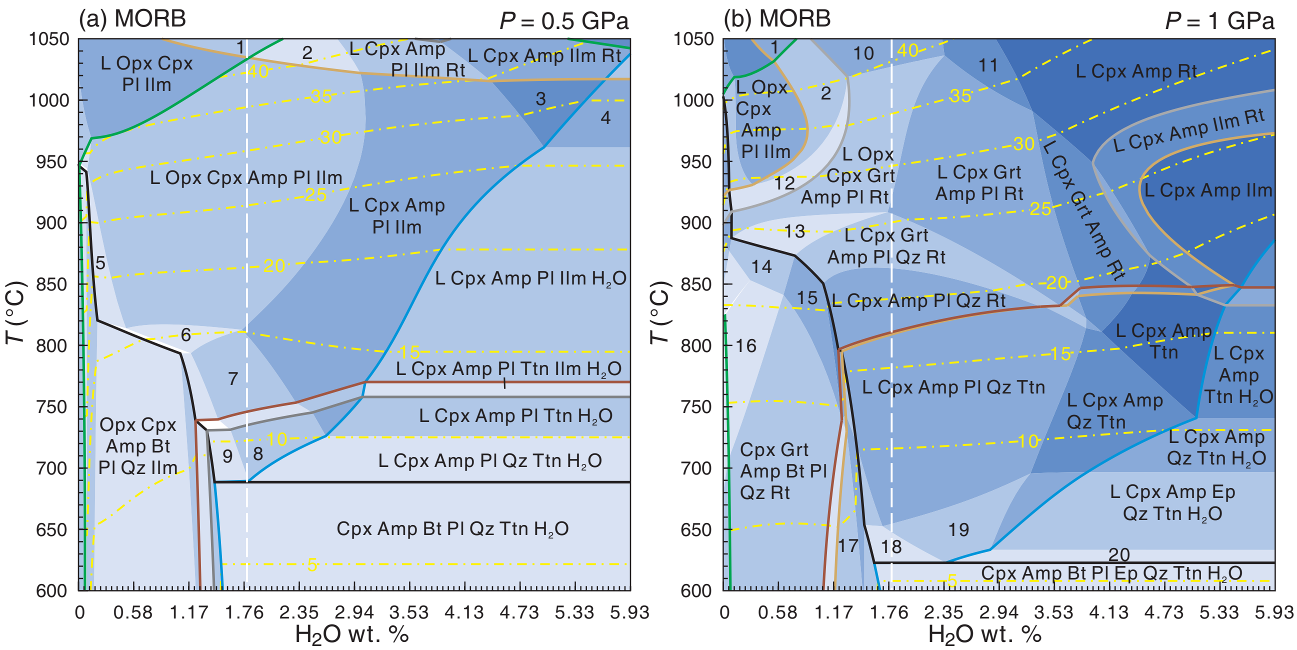

1 L Opx Cpx Pl Ilm Rt	2 L Opx Cpx Amp Pl Ilm Rt	3 L Cpx Amp Ilm	4 L Cpx Amp Ilm H_2O
5 L Opx Cpx Amp Bt Pl Ilm	6 L Opx Cpx Amp Pl Qz Ilm	7 L Cpx Amp Pl Qz Ilm	8 L Cpx Amp Pl Qz Ttn Ilm
9 L Cpx Amp Bt Pl Qz Ttn Ilm	10 L Opx Cpx Amp Pl Rt	11 L Cpx Amp Pl Rt	12 L Opx Cpx Grt Amp Pl Ilm Rt
13 L Opx Cpx Grt Amp Pl Qz Rt	14 Opx Cpx Grt Amp Pl Qz Rt	15 Cpx Grt Amp Pl Qz Rt	16 Opx Cpx Grt Amp Bt Pl Qz Rt
17 Cpx Grt Amp Bt Pl Qz Ttn	18 L Cpx Amp Bt Pl Ep Qz Ttn	19 L Cpx Amp Pl Ep Qz Ttn	20 L Cpx Amp Pl Ep Qz Ttn H_2O

Fig. 5

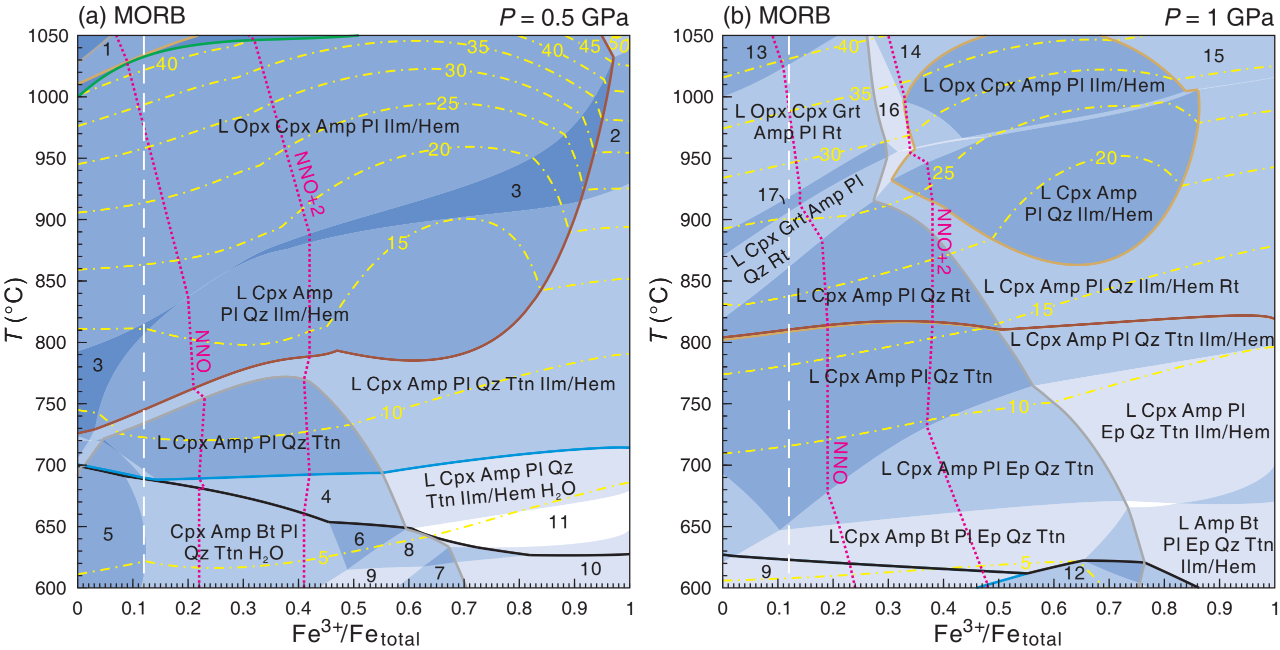

1 L Opx Cpx Pl Ilm/Hem Rt
2 L Cpx Amp Pl Ttn Ilm/Hem
3 L Cpx Amp Pl Ilm/Hem
4 L Cpx Amp Pl Qz Ttn H_2O
5 Amp Bt Pl Qz Ttn H_2O
6 Cpx Amp Pl Qz Ttn H_2O
7 Amp Bt Pl Ep Qz Ttn H_2O
8 Cpx Amp Pl Ep Qz Ttn H_2O
9 Cpx Amp Bt Pl Ep Qz Ttn H_2O
10 Amp Bt Pl Ep Qz Ttn Ilm/Hem H_2O
11 L Cpx Amp Pl Ep Qz Ttn Ilm/Hem H_2O
12 Cpx Amp Bt Pl Ep Qz Ttn
13 L Opx Cpx Amp Pl Rt
14 L Opx Cpx Amp Pl Ilm/Hem Rt
15 L Opx Cpx Amp Pl Ilm/Hem Rt
16 L Opx Cpx Grt Amp Pl Ilm/Hem Rt
17 L Cpx Grt Amp Pl Rt

DOI: https://doi.org/10.2138/am-2020-7409. http://www.minsocam.org/

Fig. 6

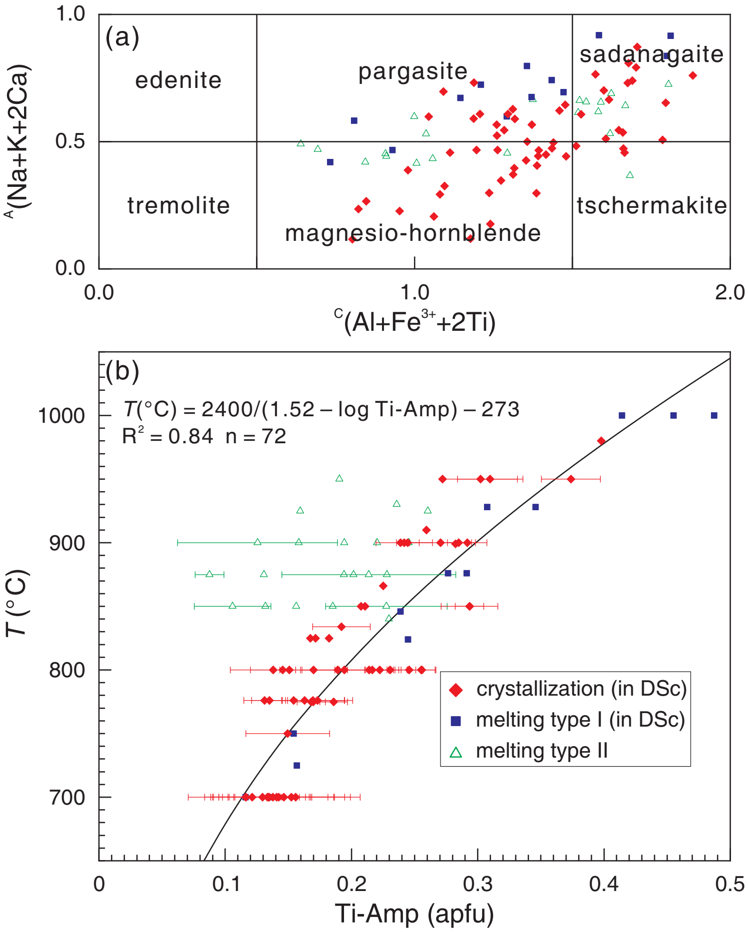

This is the peer-reviewed, final accepted version for American Mineralogist, published by the Mineralogical Society of America.
The published version is subject to change. Cite as Authors (Year) Title. American Mineralogist, in press.
DOI: https://doi.org/10.2138/am-2020-7409. http://www.minsocam.org/

Fig. 7

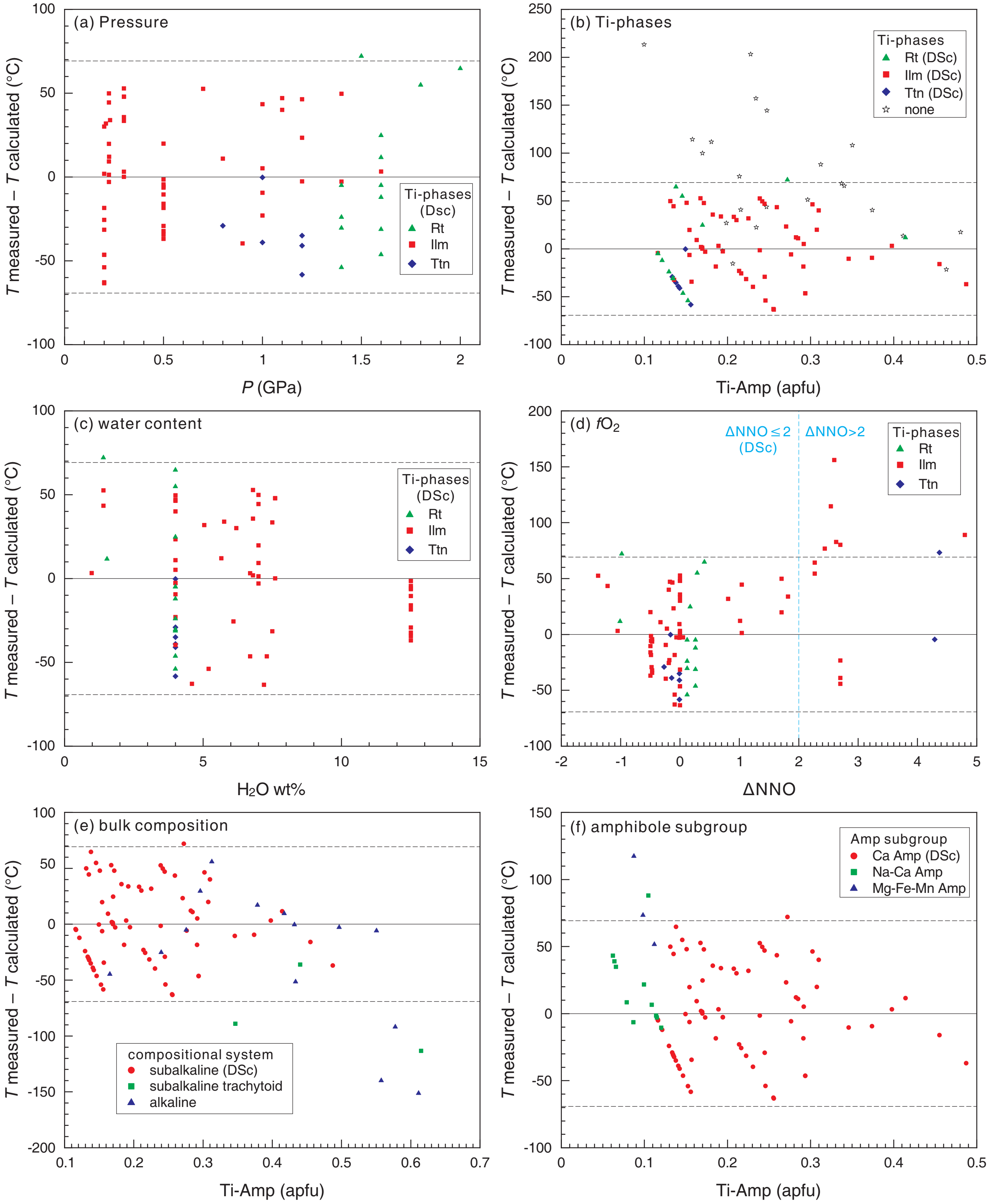

DOI: https://doi.org/10.2138/am-2020-7409. http://www.minsocam.org/

Fig. 8

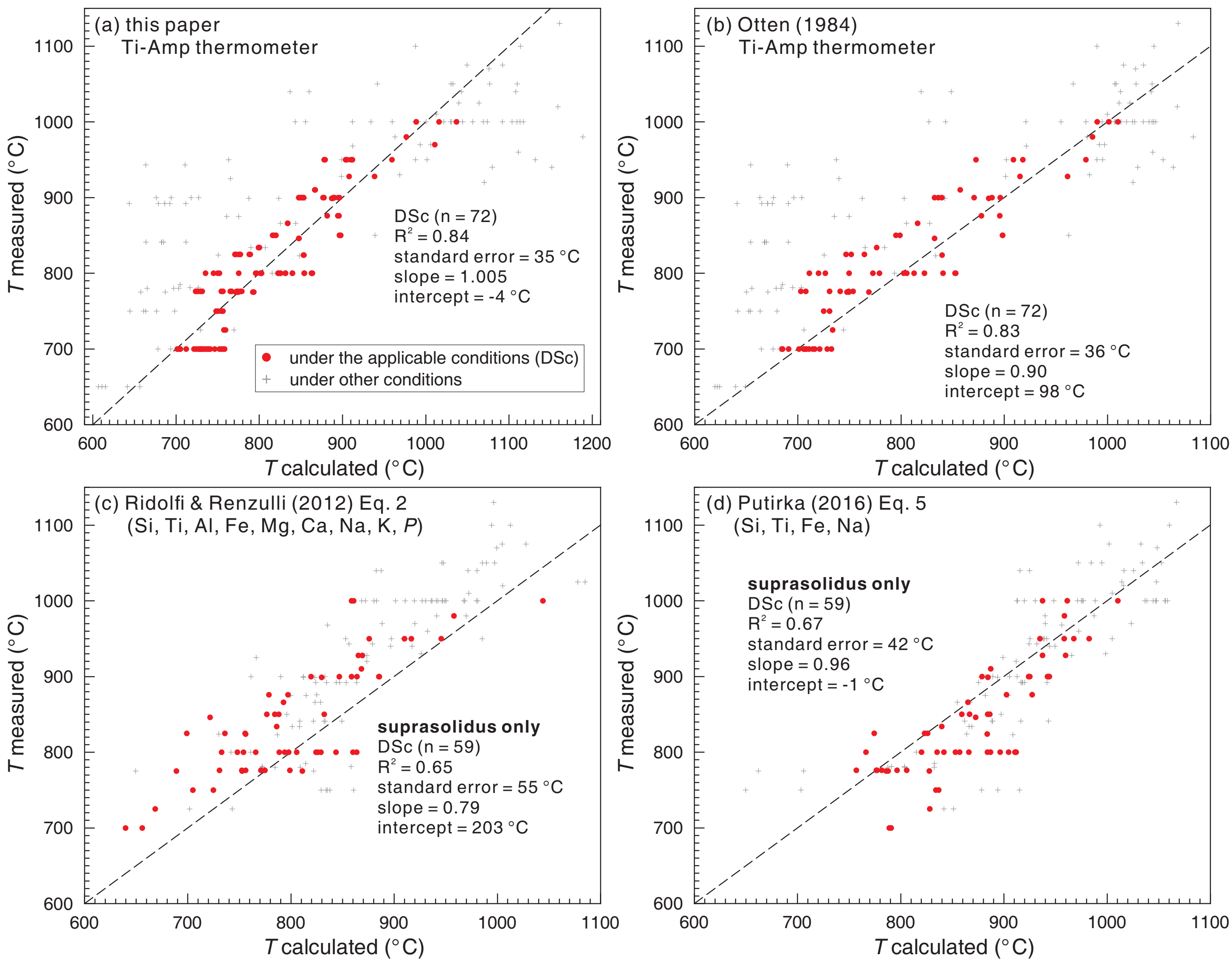

Fig. 9

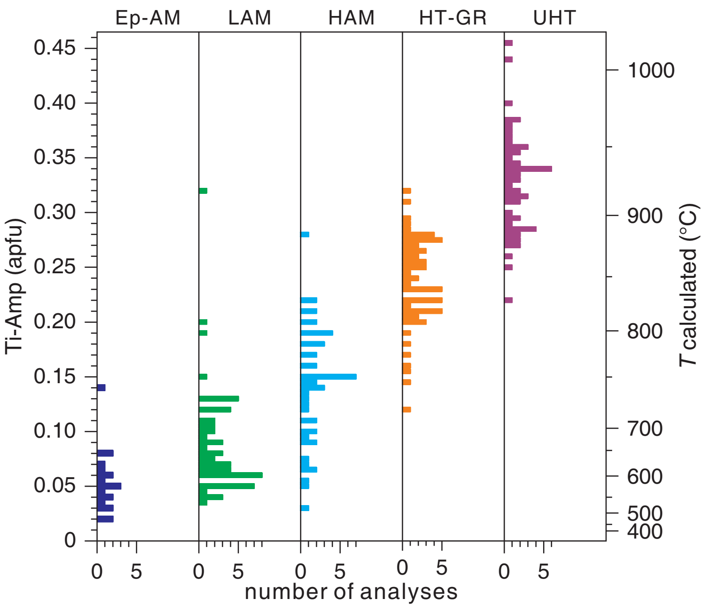
Ep-AM
LAM
HAM
HT-GR
UHT
Ti-Amp (apfu)
0.45
0.40
0.35
0.30
0.25
0.20
0.15
0.10
0.05
0
1000
900
800
700
600
500
400
T calculated (°C)
0 5
number of analyses

Fig. 10

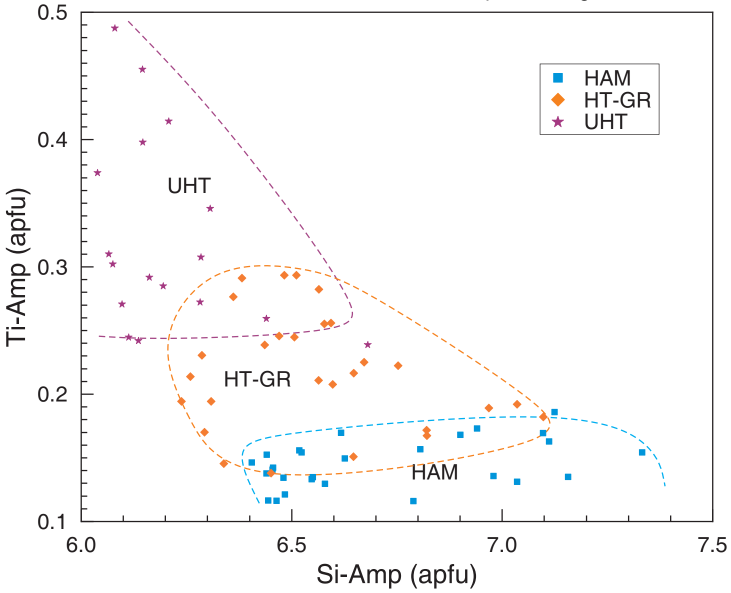
HAM
HT-GR
UHT
UHT
HT-GR
HAM
Ti-Amp (apfu)
Si-Amp (apfu)
0.5
0.4
0.3
0.2
0.1
6.0
6.5
7.0
7.5